Proceedings of the Mustansiriyah International Conference on Applied Physics (MICAP-2021)

Tri-calcium Phosphate (Nanoparticles/Nanofibers)/PVA for Bone Tissue Engineering

Furqan S. Hashim*, Mukhlis M. Ismail and Wafaa A. Hussain

Department of Applied Sciences, University of Technology, Baghdad, Iraq

Doi: 10.12693/APhysPolA.140.337 *e-mail: as.18.22@grad.uotechnology.edu.iq

Porous poly (vinyl alcohol) scaffold samples were fabricated using nanoparticles and nano-fibers of tri-calcium phosphate, which were added separately to the scaffolds with two ratios 0.05 and 0.25, respectively. Then, the results obtained were compared. The surface morphology and spectrum were examined by scanning electron microscope and Fourier transform infrared spectroscopy. The phase composition by X-ray diffraction was also examined to prove the bioactivity of the scaffold. The biodegradation, mechanical properties, porosity, density, and swelling were also tested. The impact of the strength values was enhanced significantly from 3.89 to 13.24 kJ/m^2 by using the nano-fibers of tri-calcium phosphate. However, the porosity of the tri-calcium phosphate nano-particles was higher than the tri-calcium phosphate nano-fibers by up to 62%. In fact, the porosity values in nano-fibers tri-calcium phosphate were also acceptable in comparison with the natural human bone. The samples show the highest percentage of 43% in losing weight in the G5 after incubation in phosphate buffer saline for the biodegradation test.

topics: bone tissue engineering, PVA scaffold, nanoparticles, nano fibers

1. Introduction

Tissue engineering aims to treat the damaged tissue by replacing it with complex three-dimensional tissues. The properties of bioactivity and biodegradation are considered to be the two most important characteristic features that biomaterials must possess to be suitable for use as a bone scaffold. This characteristic feature can facilitate the process of replacement of the scaffold with regenerative tissue and stimulate the body to heal itself [1, 2]. Moreover, the main requirements for scaffolds to be designed are discerned with large surface area, and its structure has interconnected pores and high porosity. It is confirmed that the interconnected pores in the scaffolds play a very effective role in cell nutrition, proliferation, and migration for tissue vascularization and formation of new tissues. However, there is a decrease in the mechanical properties with increasing porosity. There are many polymers scouted for different tissue engineering applications such as hydrogels and hydrophobic polymers [3].

Porous poly (vinyl alcohol) (PVA) is a biocompatible water-soluble polymer with non-toxic properties. The PVA has hydroxyl groups which are present in the repeating units. Thus, hygrogen bonds can be formed [4]. A bioceramic such as (TCP) could be incorporation with the PVA hydrogel to enhance the mechanical properties and to simulate the tissue structure and chemical composition of the natural bone [5]. The tri-calcium phosphate (TCP) and hydroxyapatite (HA) are phases of calcium phosphate which have the same mineral constituents as the natural bones and can easily bond to the bone. Also, calcium and phosphate ions can enhance osteogenesis [6, 7]. In addition, the latest work [8] shows that the calcium phosphate whiskers can be used in improving the mechanical properties of polymers. The effects of hydroxyapatite whiskers have been investigated to reinforce the mechanical properties of the polymer, and it was found that tensile strength and elastic modulus can increase effectively [6–8]. It is known that many materials can be synthesized as fibers. However, biocompatible non-toxic whiskers and fibers preparation remain as an important assignment. For example, whiskers of asbestos which have been used many times are now known to be very hazardous and highly carcinogenic [9].

The most common bioactive materials that attract significant attention are calcium phosphate and bioactive glass — widely used in bone tissue engineering. In particular, the composition of calcium phosphate which is very close to the bone tissue mineral part, makes it more traditional for bone graft substitution. However, their performances could still be improved [10]. The sulfuric acid is used as a catalyzer, while citric acid is chosen due to its structure of multi-carboxylic between the hydroxyl groups on the PVA and the carboxyl

groups on citric acid, the esterification could take place [11, 12]. H. Mahnama et. al [13] prepared a PVA scaffold with gelatin (Gel) and investigated the effect of Gel/PVA ratio, polymer concentration, swelling ratio, biodegradation, and the ratio of glutaraldehyde/gelatin on the morphology of pores. The results show that the scaffolds have uniform distribution of pore sizes and are almost degraded in 28 days, but the swelling ratio decreases noticeably as the polymer concentration increases. This is because of lower porosity and interconnectivity, and also because of small pore sizes.

Bhowmick et.al [14], studies the effect of zirconium oxide (ZrO_2) nanoparticles on a composite of chitosan (CTS), poly (vinyl alcohol), and hydroxyapatite (HAP). It was noticed, that the composites had interconnected porous structures with porosities in the range of human cancellous bone. These porous composites have a reduction in aqueous and SBF swelling ability with increasing nano-HAP–ZrO_2. Costa et al. [1] used the sol-gel route to prepare hybrid porous PVA/bioactive glass with partially and fully hydrolyzed PVA. From the results of surface morphology obtained with SEM, the scaffolds appeared as the macro-porous structures having pore sizes ranged from 50 to 600 μm. Hybrid polyvinyl alcohol/bioglass foams need to be very well combined to allow the control of foaming and gelatin. Such system has the potential to be used in bone tissue engineering, but further studies should be conducted.

Porous PVA foams are considered as potential biopolymers and can be utilized for bone tissue engineering. However, their lower mechanical strength limits their biological applications. This work aims to enhance the mechanical and biological properties of the scaffolds. The scaffolds as bone tissue were manufactured from PVA, nano-particles of tri-calcium phosphate (NP-TCP), and nano-fibers of tri-calcium phosphate (NF-TCP) with two ratios (0.05, 0.25), in addition to sulfuric acid as a catalizer, citric acid, and NACL to finally formaldehyde. The in vitro tests of biodegradation and bioactivity have been performed. The Fourier transform-infrared spectroscopy (FTIR), scanning electron microscope (SEM), and X-ray diffraction (XRD) are carried out on all samples. The flexural strength, impact of strength, porosity, density, and swelling ratio are also examined. The mechanical properties highly increased with NF-TCP, the impact of strength values are enhanced significantly and raised from 3.89 to 13.24 kJ/m^2. The usage of the two different forms of TCP (NP & NF) with a different ratio is to reach the best medical applications by enhancing biodegradation and bioactivity.

2. Materials and methods

The nanoparticles (NP) and nano-fibers (NF) of tri-calcium phosphate (TCP) (Ying Tong Chem and Tech, LTD, density 3.14 g/cm^3, China) were added with ratios of $(0, 0.05, 0.25)$ with respect to the weight of 4 g of PVA (Central Drug House, molecular weight 13000–23000, viscosity 3.5–4.5, Hydrolysis 87–89%, pH 4.5–6.5, India) after dissolving in 24 ml distilled water with a heating stirrer at 85°C for 10 min as shown in Table I.

TABLE I

The proportions of adding NP-TCP and NF-TCP to the 4 gm. of polyvinyl alcohol (PVA).

Additives	Name	Percentage [%]
none	G1	0
nanoparticles TCP	G2	0.05
	G3	0.25
nanofibers TCP	G4	0.05
	G5	0.25

For catalizer, the 8 ml of sulfuric acid (Central Drug House, molecular weight 98.08, India) was used, citric acid (Central Drug House, molecular weight 192.13, India) of 24 g added to the mixture for creation of esterification bonding. The 24 g of NaCl (Central Drug House, molecular weight 58.44, pH 5–8, India) were added to the mixture. Finally, the formaldehyde (Central Drug House, molecular weight 30.03, India) of 3 ml was added to the mixture. The mixture was injected into the metal molds for ASTM tests and cured at 85°C for 45 min.

3. Method

The impact of strength test was carried out with the chirpy impact test machine for un-notched samples (Impact tester N, 43-1). The pendulum with 2 kg of weight was released from a specific height to record the zero reading. The pendulum was dropped again after placing the sample horizontally on the carrier and records the impact on the sample. The impact of strength (IS) [kJ/m^2] was calculated [15] as

$$\mathrm{IS} = \frac{E - \text{zero reading}}{bd}, \tag{1}$$

where the energy of fracture is represented by E. The test sample width and thickness are denoted by (b) and (d), respectively.

The flexural strength was carried out by (Instron, 1195), a tensile testing machine. The distance between two parallels supporting the specimens was equal to 50 mm. The load was applied to the center of the sample of the weight of 20 kN until it was broken, and with a speed of 5 mm/min. The flexural strength (FS) [MPa] is determined by [15]

$$FS = \frac{3PL}{2bd^2}, \tag{2}$$

where P [N] denotes the maximum load , and L is the separation distance.

The density (ρ) and porosity (p) of the foam samples were measured by the liquid displacement method and calculated, respectively, as

$$\rho = \frac{W}{V_2 - V_3} \tag{3}$$

and

$$p = \frac{V_1 - V_3}{V_2 - V_3} \times 100\%. \tag{4}$$

Here, the weight of the dry sample is W and the volume of ethanol is V_1. The total volume of the sample and ethanol, after immersing the sample into ethanol for 24 h to saturation, is V_2. Finally, V_3 is the residual ethanol volume after the sample removal from the ethanol [14].

The aqueous swelling ratio was measured by immersing the samples in distilled water at specified time intervals after recording their dry weight (W_d). The samples were then removed from water and carefully dried up by filter paper to remove excess water and record their wet weight (W_w). The swelling index was calculated accordingly

$$\text{Swelling index} = \frac{W_w - W_d}{W_d} \times 100\%. \tag{5}$$

The biodegradation test was carried out by incubating the samples in phosphate buffer saline (PBS) (pH 7.4, concentration of 0.1 M) at 37°C for 1 week. The samples were removed and dried at 50°C overnight. The mass loss [%] was calculated accordingly

$$\text{mass loss} = \frac{W_0 - W_t}{W_0} \times 100\%, \tag{6}$$

where W_0 is the initial mass, W_t is the mass after incubated in PBS. This calculation was repeated for 4 weeks for the degradation test.

The bioactivity was tested by immersing the samples in Ringer's solution for 21 days at 37°C in water bath. Then, they are removed from the Ringer's solutions and dried at room temperature. The XRD with Cu K_α ($\lambda = 1.54$ Å) at 40 kV and 30 mA were employed to confirm the presence of tri-calcium phosphate as a sign of bioactivity. Ionic substitution and differentiation between different levels of relative crystallization were identified by the FTIR machine (SHIMADZU IRFFINITY) which records in the wave number range from 400 to 4000 cm^{-1}. The sample surface morphology was examined by SEM (FEI Quanta 450) to obtain the size of the pores.

4. Results and discussion

The morphology of surfaces with NP-TCP and NF-TCP added to scaffolds are shown in Fig. 1a and 1b, respectively. A spherical NP powder with an average diameter of 43.4 nm is observed in Fig. 1a. The average diameter of NF-TCP is 40.3 nm and is shown in Fig. 1b.

Figure 2 gives SEM micrographs illustrating surface morphology of PVA scaffold samples with and without different additives. The observed morphologies of the scaffolds vary with various additives.

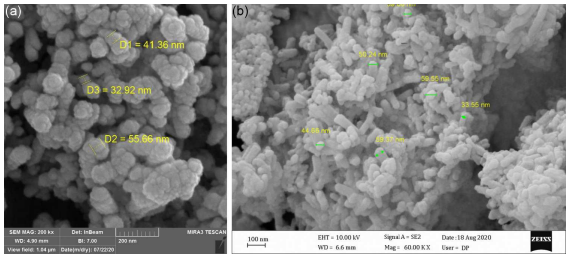

Fig. 1. Scanning electron micrographs of the TCP used in scaffolds (a) NP-TCP, (b) NF-TCP.

The porosity and pore sizes are dependent on the composition of the scaffold and on the concentration of the additives. It can be seen that the samples have an irregular and overlapping porous structure, which increases the porosity of the sample and its susceptibility to biodegradation, but also has an opposite effect on the mechanical properties, restricting the addition of more TCP. Figure 2c and d shows G2 with increased NP-TCP content, and G3 with increased NP-TCP content is shown in Fig. 2e and f. If G2 and G3 can destroy the crystalline cross-linking points, then the number and size of the pores inside the scaffold structure increases compared with G1 which contain PVA without additives. The average diameter observed in NP-TCP is up to 350 ± 40 μm. The micropores enable the transport of nutrients and oxygen that are required for cell survival. The morphology of samples with NF-TCP additives differs from that of NP-TCP particles additives, whereas the pore size became smaller with the average diameter of about 135 ± 40 μm in NF-TCP samples as compared to NP-TCP samples. This happens because of large area of NF compared to NP which leads to increased density and decreased porosity, as shown in Fig. 2g, h and 2i, j, respectively. The cancellous bone has 300–600μm diameter pores and the cortical bone has 10–50 μm diameter pores [16].

Figure 3 illustrates the FTIR spectra of PVA scaffolds nanocomposite. The peak in scaffold G1 (without additives) has a broad band of the hydroxyl O–H bond between 3100 and 3600 cm^{-1} and the absorption peak located at 3493.68 cm^{-1} is for (-N–H-) bond. For G2 and G3 samples, the peaks of the sp^3 C–H alkyl bond appear at 2924, 2958, 2964 cm^{-1}, respectively. Both G4 and G5 show the same strength in broad peaks at 3100 and 3740 cm^{-1}, respectively, and are assigned to the characteristic stretching peaks of hydroxyl (O–H) reflecting the intramolecular charcter of the hydrogen bond. The peaks of C=C appear at 1640–1680 cm^{-1}. The PVA group of the vinyl acetate remains non-hydrolyzed and is observed by the appearance of peaks at 1124–1174 cm^{-1}, which are due to stretching vibrations of C=O and C–O, respectively. The absorption peak appeared at 1730–1732 cm^{-1}.

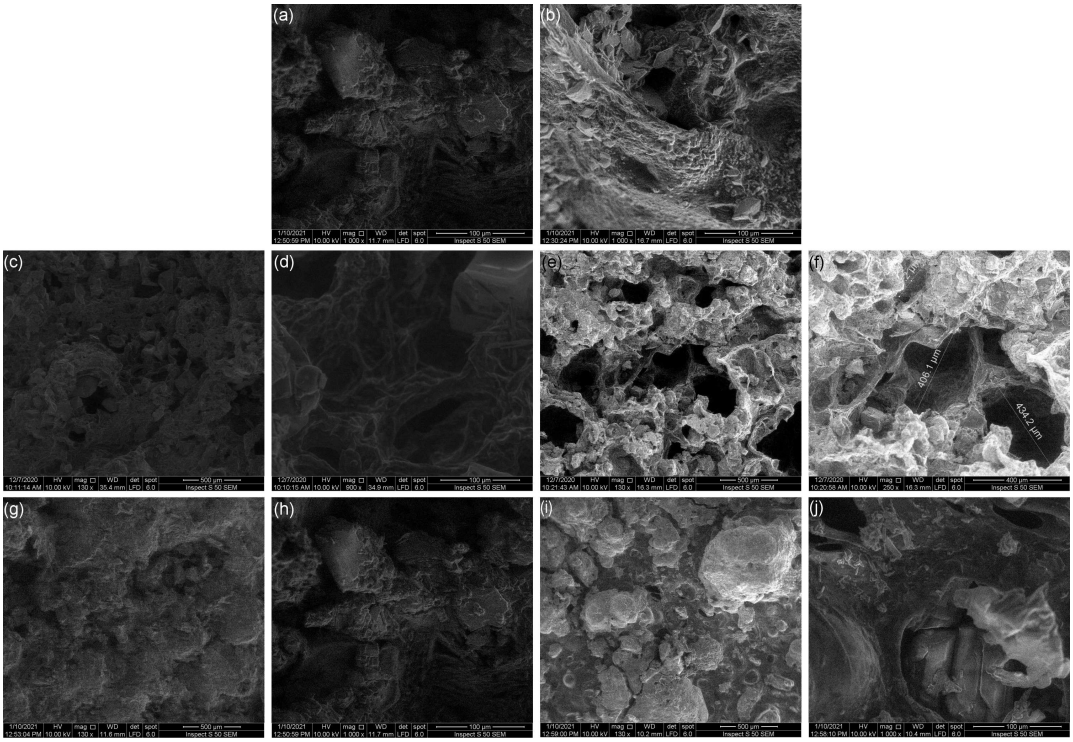

Fig. 2. Scanning electron micrographs (SEM) of: (a, b) G1: PVA scaffold without additive, (c, d) G2: 0.05% NP-TCP, (e, f) G3: 0.25% NP-TCP Particles, (g, h) G4: 0.05% NF-TCP, (i, j) G5: 0.25% NF-TCP.

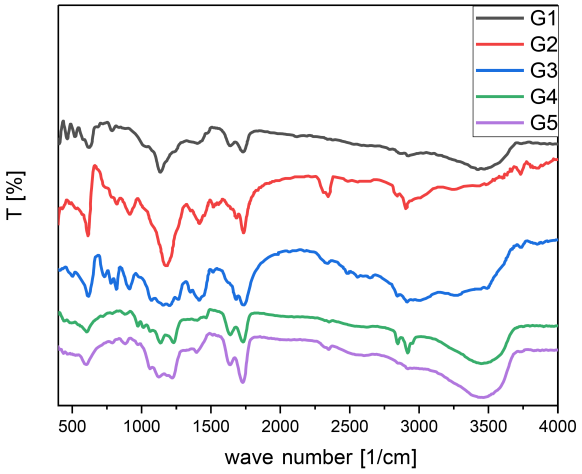

Fig. 3. FTIR spectra of PVA scaffold with different additives.

The band ranging from 2900 to 2950 cm^{-1} represents symmetric and asymmetric stretching modes related to $–CH_2$ groups [17]. Also, new PVA bands appeared in the range 1411 and 1350 cm^{-1} that represent C–H bending modes. In the FTIR spectrum of the PVA, the peaks at 1174, 1163, 1151, and 1068 cm^{-1} remain unchanged, and are assigned to stretching vibrations of C–O–C–O–C. Finally, the O–H bending vibration that appeared at 1640 cm^{-1} is shown also in the FTIR spectrum related to the PVA.

The porosity affects cell proliferation and adhesion. According to Table II, the porosity of PVA scaffold samples is increased as the additives increase. The PVA contains many hydroxyl groups and it is easy to form hydrogen bonding, resulting in lower porosity. After incorporation of both TCP particles and fibers, the porosity of the scaffold increases and reaches 62% and 58% respectively. The reason for the decrease in the porosity values of the NF-TCP compared to the NP-TCP is due to the fact that the NF-TCP takes up a larger area and therefore its density is larger compared to the NP-TCP. The porosity percentage of human spongy bone has the value of 50–90 [18]. Thus, the porosity values in fibers are also acceptable. The porosity decreases with increasing packing density of the scaffolds and fiber diameters [19]. Often, there is an inverse relation between porosity and density, as with increasing porosity the density decreases and vice versa. Tables II and III show the increasing and decreasing porosity and density values with increasing the addition ratio respectively.

The mechanical properties of the porous scaffold should be enhanced. However, the low strength and brittleness of TCP have limited its wide application in hard tissue implants [20]. The TCP is used like fibers, and the results are compared in Table IV. Incorporation of NP to β-TCP in PVA scaffold causes a reduction in impact strength and this reduction increases with the increase of powder addition, however, it is clear that the impact strength increased with NF-TCP to 13.24 MPa in G5.

TABLE II
Statistical values of porosity percentage.

Group No.	Avg. pore size [μm]	Porosity [%]			
		Mean	Min	Max	SD
G1	26.9	47	41	53	2.3
G2	72.9	52	46	55	3.4
G3	340.5	62	55	68	4.6
G4	27.9	50	44	57	6.1
G5	135.2	58	50	61	5.4

TABLE III
Statistical values of density.

Group No.	Density [g/cm^3]			
	Mean	Min	Max	SD
G1	0.51	0.47	0.56	0.03
G2	0.44	0.39	0.48	0.05
G3	0.38	0.31	0.45	0.04
G4	0.5	0.43	0.59	0.08
G5	0.43	0.39	0.5	0.07

TABLE IV
Statistical impact strength.

Group No.	Impact strength [kJ/m^2]			
	Mean	Min	Max	SD
G1	3.89	3.54	4.15	0.31
G2	3.36	3.19	3.5	0.16
G3	2.77	2.63	2.97	0.09
G4	9.42	8.98	10.1	1.30
G5	13.24	12.78	14	3.4

The flexural strength results recorded a significant decrease when using NP-TCP. While the results are different when using the NF-TCP, the flexural strength value increases with the increase in the percentage of additions in G4 and G5, as shown in Table V. By increasing the ratio of fibers, we can obtain higher values of the flexural strength. The mechanical properties are increased by using the fibers because the fibers absorb the shock or the load applied to the sample.

Aqueous swelling tests of scaffolds have been carried out to obtain the water uptake capabilities. The aqueous swelling reaches equilibrium after 24 h and is highly increased for all samples, as shown in Fig. 4. This can be traced back to the penetration of water and the physical bonding with water molecules resulting from hydroxyapatite and unreacted hydrophilicity of the PVA [19]. There are no relevant differences observed when using different ratios of the TCP particles. The same rise is obtained with the TCP nano-fibers as well as the TCP nano-particles, however increase in the aqueous swelling in high G5 containing nano-fibers is relatively slower than in other samples. These results indicate that the optimum medium uptake will help

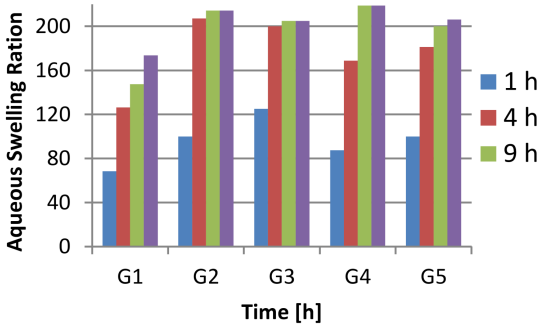

Fig. 4. The aqueous swelling ration of PVA samples with different additives of particles and fibers TCP.

TABLE V
Statistical flexural strength.

Group No.	Flexural strength [MPa]			
	Mean	Min	Max	SD
G1	6.1	5.8	6.3	0.28
G2	5.75	5.51	6	0.42
G3	1.41	1.23	1.68	0.07
G4	6.3	6.06	6.42	0.16
G5	7.2	6.56	7.45	0.54

in the attachment and proliferation of cells on the scaffold because of blood's hydrophilic nature. This, in fact, can lead to improved delivery of scaffolds' drugs and nutrients to cultured cells [21].

The PVA scaffold sample shows a 43% weight loss which is the highest weight loss in G5 after four weeks of incubation in phosphate buffer saline (PBS), as shown in Fig. 5. The samples have more amorphous domains as the XRD results show (see Fig. 6). The mobile chains will allow water to penetrate through it easier than through dense crystalline regions, so the scaffold samples are expected to undergo hydrolytic degradation [22]. In physiological content, β-TCP is degraded by chemical dissolution and by its effects on the bone remodeling process [23]. Hence, the PVA scaffold composite sample is considered to be an ideal biodegradable material for use as a scaffold in bone tissue engineering.

Bioactivity test of samples was performed with XRD to confirm the formation and presence of TCP. The X-ray diffraction (XRD) has been carried out to get scaffold's spectra before and after immersion in Ringer's solution and to describe phase changes. The results showed that the XRD pattern changed considerably after immersing the sample in solution for 21 days, as shown in Fig. 6. We notice also that G3 and G5 samples before immersion have peaks at $2\theta = 28.36°$, $29.24°$, $29.27°$, $31.16°$ and $31.48°$ which refer to tri-calcium phosphate nanoparticles [24, 25], and the diffraction pattern with semi-crystalline nature around $2\theta = 22°$ and $22.72°$, due to the presence of PVA [26].

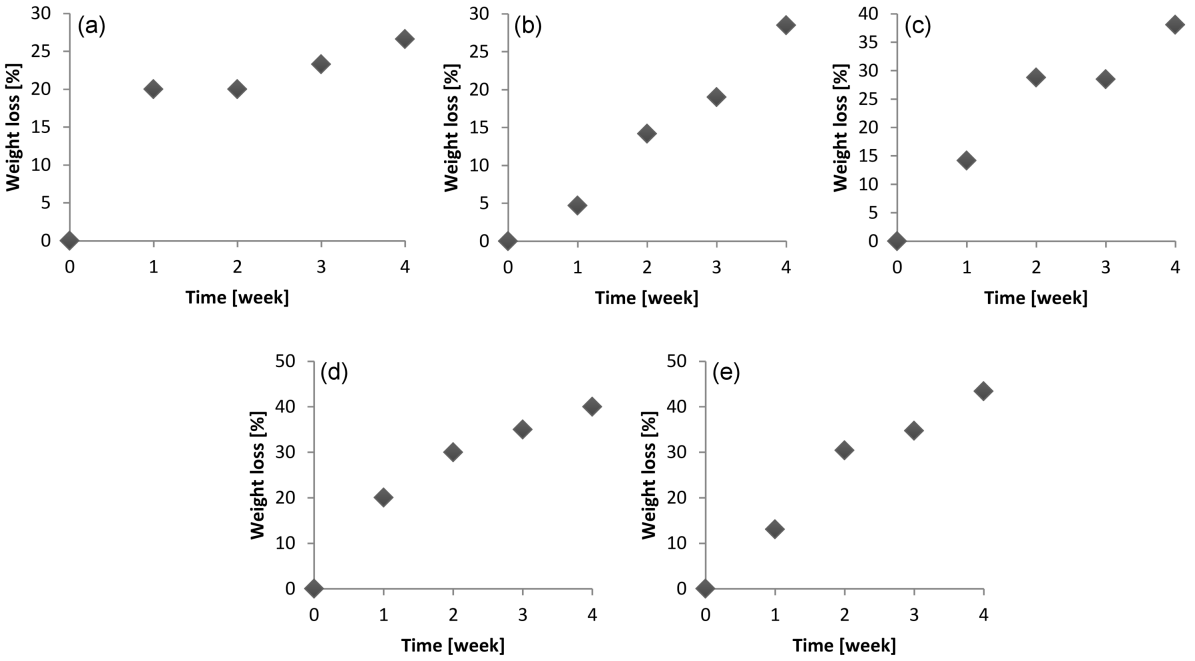

Fig. 5. Biodegradation indicated by weight loss [%] of scaffold samples.

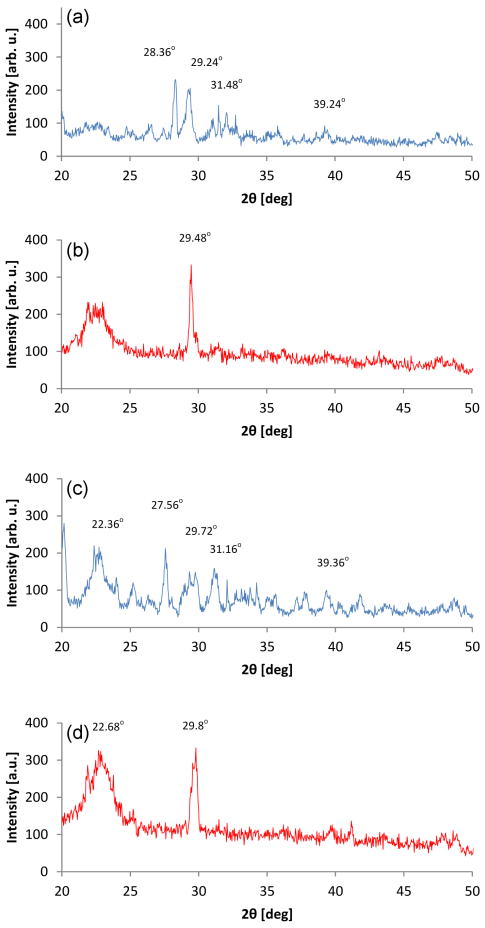

Fig. 6. The XRD patterns of the samples with high percentage of additive, (G3: NP-TCP) and (G5: NF-TCP).

After immersion in Ranger's solution for 21 days, we notice that all peaks disappear, except the peak at $2\theta = 29.48°$ in G3 which represents the tri-calcium phosphate present in the natural bone [21]. With regard to G5, we notice a magnification of the peak at $2\theta = 29.32°$ of tri-calcium phosphate and its drag up to $2\theta = 29.8°$. Therefore, the sample is biologically effective for the bone because TCP is the main material in the natural bone. The peaks representing the structure of calcium phosphate are similar to those present in the human bone tissue, thus maintaining similarity in the pattern [27]. It is likely that the rest of the peaks will disappear due to their biodegradation after this period and the sample will be covered with TCP instead.

5. Conclusions

In addition to what is shown, TCP as powder or fiber added to PVA affects porosity and pore size. The porosity of the nanoparticles of tri-calcium phosphate NP-TCP is higher than the nanofibers of tri-calcium phosphate NF-TCP. The porosity values in NF-TCP are also acceptable. The pore size increases when NP-TCP is used, while it is decreased if NF-TCP is used instead. The mechanical strength values increase significantly when NF-TCP is used, namely the strength values increase from 3.89 to 13.24 kJ/m^2, after they have decreased when using the NP-TCP. The scaffolds show good biodegradation and bioactivity. The results confirm the presence and growth of the peak of calcium phosphate in the composite material, which is also present in human bone tissue, thus maintaining similarity in the pattern.

References

[1] V.C. Costa, H.S. Costa, W.L. Vasconcelos, M.D. M. Pereira, R.L. Oréfice, H.S. Mansur, *Mater. Res* **10**, 21 (2007).

[2] M.S. Enayati, T. Behzad, P. Sajkiewicz, M. Rafienia, R. Bagheri, L. Ghasemi-Mobarakeh, S.H. Bonakdar, *J. Biomed. Mater. Res. A* **106**, 1111 (2018).

[3] A.S. Hoffman, *Adv. Drug Deliv. Rev.* **64**, 18 (2012).

[4] S. Nkhwa, K.F. Lauriaga, E. Kemal, S. Deb, *Conf. Paper Sci.* **2014**, 403472 (2014).

[5] M. Xu, M. Qin, X. Zhang, X. Zhang, J. Li, Y. Hu, D. Huang, *J. Biomater. Sci. Polym. Ed.* **31**, 816 (2020).

[6] C. Shuai, Y. Cao, C. Gao, P. Feng, T. Xiao, S. Peng, *BioMed Res. Int.* **40**, 8469 (2015).

[7] W.A. Hussain, E.H. Al-Mosawe, M.M. Ismail, L.H. Alwan, *J. Biomim. Biomater. Biomed. Eng.* **49**, 101 (2021).

[8] S.U. Maheshwari, V.K. Samuel, N. Nagiah, *Ceram Int.* **40**, 8469 (2014).

[9] S. Jalota, S.B. Bhaduri, A.C. Tas, *J. Biomed. Mat. Res. A* **78A**, 481 (2006).

[10] J.V. Rau, I. Antoniac, G. Cama, V.S. Komlev, A. Ravaglioli, *BioMed Res. Int.* **2016**, 3741428 (2016).

[11] R. Shi, J. Bi, Z. Zhang, A. Zhu, D. Chen, X. Zhou, W. Tian, *Carbohydr. Polym.* **74**, 763 (2008).

[12] W.C. Hsieh, J.J. Liau, *Carbohydrate polymers* **98**, 574 (2013).

[13] H. Mahnama, S. Dadbin, M. Frounchi, S. Rajabi, *Artif. Cells. Nanomed. Biotechnol.* **45**, 928 (2017).

[14] A. Bhowmick, N. Pramanik, T. Mitra, A. Gnanamani, M. Das, P.P. Kundu, *New J. Chem.* **41**, 7524 (2017).

[15] W. A. Hussain, B.A.M. Bader, M.Y. Slew, L.H. Alwan, *Mat. Sci. Forum* **1002**, 340 (2020).

[16] S. Lee, M. Porter, S. Wasko, G. Lau, P.Y. Chen, E.E. Novitskaya, J. McKittrick, *MRS Online Proc. Library* **1418**, 177 (2012).

[17] B. Xue, J. Deng, J. Zhang, *RSC Adv.* **6**, 7653 (2016).

[18] V. Santacruz-Vázquez, C. Santacruz-Vázquez, J.O. Laguna Cortés, *J. Vitae*, 22 (2), 75-86 (2015). .

[19] S. Soliman, S. Sant, J.W. Nichol, M. Khabiry, E. Traversa, A. Khademhosseini, *J. Biomed. Mater. Res. A* **96**, 566 (2011).

[20] S. Sakka, J. Bouaziz, F.B. Ayed, in: *Advances in Biomaterials Science and Biomedical Applications*, Intech 2013.

[21] A.A. Ashraf, S.M. Zebarjad, M.J. Hadianfard, *J. Mater. Res. Technol.* **8**, 3149 (2019).

[22] L.V. Thomas, U. Arun, S. Remya, P.D. Nair, *J. Mater. Sci. Mater. Med.* **20**, 259 (2009).

[23] S.H. Huang, Y.J. Chen, C.T. Kao, C.C. Lin, T.H. Huang, M.Y. Shie, *J. Dent. Sci.* **10**, 282 (2015).

[24] M. Ebrahimi, M.G. Botelho, *Data Brief* **10**, 93 (2017).

[25] B. Sarikaya, H.M. Aydin, *BioMed Res. Int.* **2015**, 576532 (2015).

[26] S. Mahendia, A.K. Tomar, R.P. Chahal, P. Goyal, S. Kumar, *J. Phys. D Appl. Phys.* **44**, 205105 (2011).

[27] C.J.C. Perera, M.G.C. Baas, G.A.A. Lara, S.I.R. Borges, A.L.R. Guzmán, I.F. Cervantes, N.R. Fuentes, *Health Technol.* **10**, 423 (2020).